



Full length article

Bioengineering strategy to promote CNS nerve growth and regeneration via chronic glutamate signaling

Karen Chang^{a,b}, Jih-Guang Wu^c, Tien-Li Ma^c, Sheng-Hao Hsu^d, Kin-Sang Cho^a,
Zicheng Yu^{a,e}, Anton Lennikov^{a,b}, Ajay Ashok^{a,b}, Aishwarya Rajagopalan^{a,f}, Min-Huey Chen^d,
Wei-Fang Su^c, Tor Paaske Utheim^{b,g,h}, Dong Feng Chen^{a,*}

^a Schepens Eye Research Institute of Massachusetts Eye and Ear, Department of Ophthalmology, Harvard Medical School, Boston, MA, USA

^b Department of Medical Biochemistry, Oslo University Hospital, Oslo, Norway

^c Department of Materials Science and Engineering, National Taiwan University, Taipei, Taiwan

^d Graduate Institute of Clinical Dentistry, School of Dentistry, National Taiwan University, Taipei, Taiwan

^e MRC Human Genetics Unit, Institute of Genetics and Cancer, The University of Edinburgh, Edinburgh, UK

^f Department of Biological Sciences, College of Agriculture and Life Sciences, Cornell University, Ithaca, NY, USA

^g Department of Ophthalmology, Oslo University Hospital, Oslo, Norway

^h Department of Ophthalmology, Drammen Hospital, Drammen, Norway



ARTICLE INFO

Keywords:

Electrical stimulation
Tissue engineering
Glutamate
Retinal ganglion cells
Nerve regeneration

ABSTRACT

Being part of the mature mammalian central nervous system, impairments of the retina and optic nerves caused by trauma or diseases often cannot be restored. Progressive degeneration of retinal ganglion cells (RGCs) in glaucoma and other optic neuropathies gradually leads to permanent vision loss, which currently has no cure. The purpose of this study is to develop a biocompatible scaffold to support RGC survival and guide axon growth, facilitating optic nerve repair and regeneration. We here report that electrical stimulation (ES) significantly promoted neurite outgrowth and elongation from primary RGCs, mediated through glutamate receptor signaling. To mimic prolonged glutamate stimulation and facilitate sustained nerve growth, we fabricated biocompatible poly- γ -benzyl-L-glutamate (PBG) scaffolds for controlled glutamate release. These PBG scaffolds supported RGC survival and robust long-distance nerve growth in both retinal explants and isolated RGC cultures. In contrast, control polycaprolactone (PCL) scaffolds with similar physical structures showed little benefits on RGC survival or nerve growth. Moreover, PBG scaffolds promoted the differentiation and neurite outgrowth from embryonic stem cell-derived RGC progenitors. The aligned PBG scaffold drove directed nerve elongation along the fiber alignment. Transplantation of PBG-coated biocompatible conduits induced robust optic nerve regeneration in adult mice following nerve transection. Together, the findings present the exciting possibility of driving optic nerve regeneration and RGC progenitor cell differentiation by imitating ES or glutamate signaling. PBG presents a permissive biomaterial in supporting robust and directed axon growth with promising clinical applications in the future.

Statement of Significance: We here reported compelling findings that demonstrate the potent regenerative effects of a bioengineered scaffold incorporating poly- γ -benzyl-L-glutamate (PBG) on the optic nerve. Retinal ganglion cell (RGC) axons, which form the optic nerve, are incapable of regenerating in adulthood, posing a significant hurdle in restoring vision for patients with optic nerve diseases or injuries. Built upon the finding that electrical stimulation promotes RGC axonal growth through glutamate signaling, we developed PBG scaffolds to provide sustained glutamate stimulation and showed their exceptional effects on driving directed axonal elongation in cultured RGCs and neural progenitors, as well as supporting robust optic nerve regeneration after transection *in vivo*. The findings hold great promise for reversing vision loss in patients with optic nerve conditions.

* Correspondence author.

E-mail address: Dongfeng.chen@meei.harvard.edu (D.F. Chen).

<https://doi.org/10.1016/j.actbio.2024.10.023>

Received 19 January 2024; Received in revised form 21 September 2024; Accepted 16 October 2024

Available online 18 October 2024

1742-7061/© 2024 Acta Materialia Inc. Published by Elsevier Ltd. All rights are reserved, including those for text and data mining, AI training, and similar technologies.

1. Introduction

According to the World Health Organization (WHO), in 2023, an estimated 2.2 billion people suffer from vision impairment globally. Among the leading causes of vision impairment, trauma or diseases such as diabetic retinopathy, glaucoma, and age-related macular degeneration causing retinal degeneration and optic nerve damage remains no effective cure [1,2]. As the prevalence of vision impairment is expected to increase with the growth of aging population worldwide, developing feasible treatments for retinal degenerative diseases is an urgent and imperative task [3].

The retina contains light-sensitive photoreceptors that transduce light into chemical and electrical signals. These signals pass through bipolar and amacrine cells and reach retinal ganglion cells (RGCs) in the retina. RGCs collectively convey signals into action potentials through their axons in the optic nerve, which transmit visual information to the brain [4]. Optic nerve injuries and retinal degenerative diseases often lead to the progressive death of retinal neurons, causing nerve damage and resulting in permanent vision loss. Mature mammalian RGCs have limited regenerative potential. Once the degeneration has occurred, they are unable to regrow axons and undergo apoptosis, leading to permanent vision loss [5–7].

Increasing evidence suggests that electrical stimulation (ES) has the potential to preserve retinal neurons, including RGCs [8–10], and promotes nerve regeneration in retinal degenerative disease models [11–16]. ES is also reported to protect other retinal neurons by stimulating neurotrophic factor release to increase survival and reduce apoptotic signals [13,17].

As a primary neurotransmitter of RGCs and other neurons, glutamate mediates point-to-point transmission across the synaptic cleft in excitatory synapses, conveying nerve impulses between axons and dendrites [18,19]. Additionally, it is a critical player in the majority of neuronal regulatory events, including neurogenesis, neurite outgrowth, synaptogenesis, neuron survival, and homeostasis in the mammalian nervous system [20,21]. Glutamate primarily activates two groups of receptors: ionotropic glutamate receptors (iGluRs) and metabotropic glutamate receptors (mGluRs). Elevated extracellular concentrations of glutamate, due to excessive activation of glutamate receptors, can cause excitotoxicity, leading to rapid RGC degeneration and sudden onset of ischemia, as well as contributing to chronic neurodegenerative diseases such as Alzheimer's and Huntington's diseases [21–23]. In contrast, at appropriate concentrations, glutamate is essential and plays a crucial role in promoting neural differentiation and nerve growth during development. Properly harnessing glutamate signaling could offer a potential strategy for optic nerve regeneration.

Recent research has been focusing on nerve regeneration through tissue engineering approaches, contributing to significant advancements in the field [24–26]. Tissue engineering requires a combination of cells, biocompatible scaffolds, and suitable biochemical or physicochemical signals to repair, restore, or replace damaged biological tissues [27]. In peripheral nerve regeneration, Jiang et al. constructed an artificial nerve conduit that enabled nerve regeneration across large defect gaps through new synthetic polymers [28]. However, to repair the central nervous system (CNS), such as the spinal cord, remains challenging [29,30].

In the past decade, electrospinning has intensively attracted researchers due to its versatility in fabricating fibrous structures [31–33]. This technique produces materials with a high surface-area-to-volume ratio, resulting in extensive interconnected porous networks. Electrospun fibers can be designed with various alignments and orientations for specific application requirements. In one instance, Kador et al. demonstrated a biodegradable electrospun scaffold designed to direct the growth of RGC axons radially, mimicking the natural orientation of axons in the retina [33].

In this study, we demonstrated that PBG bioscaffolds, mimicking the controlled glutamate release or glutamate signaling of ES, promote

robust neurite outgrowth and elongation. The molecular weight of PBG ranges from 200 to 300 kDa, and glutamate is immobilized as benzyl glutamate units in PBG [34,35]. We previously reported that the side chain of polybenzyl glutamate hydrolyzes into benzyl alcohol and polyglutamic acid when the polypeptide main chain remains intact during a 42-day hydrolytic degradation test [35]. The large molecular structure of PBG polymer prevents the rapid release of glutamate and glutamate-excitotoxicity at the site of transplantation. We found that the PBG scaffold with aligned fibers is biocompatible, supporting cell survival and promoting substantial growth of long neurites in primary cultured RGCs, retinal explants, and RGCPs that extended along the direction of the fibers. By imitating the environment with a bioactive scaffold for RGCs to grow on, the PBG scaffold presents a bioengineered strategy that promotes directed axon growth and may serve as a feasible treatment for restoring and preserving vision from retina degeneration and optic nerve damage.

2. Materials and methods

2.1. Animals

Adult C57BL/6J mice were purchased from Jackson's Laboratory (Stock # 000,664; Bar Harbor, ME, USA) and maintained in the Animal Facility of Schepens Eye Research Institute of Massachusetts Eye and Ear for breeding and *in vivo* transplantation purposes. All animal experiments were performed following protocols approved by the Institutional Animal Care and Use Committee of the Schepens Eye Research Institute and followed the Association for Research in Vision and Ophthalmology (ARVO) standards of using animals in research. The mice were kept in a 12-hour light/dark cycle with free access to food and water. Pups were decapitated for the isolation of retinal cells and explant cultures. Adult mice were euthanized by CO₂ asphyxiation at the experimental endpoint.

2.2. Retinal ganglion cell isolation and culture

Primary mouse retinal ganglion cells (RGCs) were isolated from the retinas of postnatal day 0–3 (P0–3) C57BL/6J mice as previously described [36–41]. All data were repeated from at least 3 independent cultures. For each culture, RGCs harvested from mouse pups of the same age were pooled and cultured in corresponding control groups. This allowed us to eliminate potential variations due to age, sex, and individual pups. Furthermore, no significant differences were found in the survival rates of primary RGCs isolated between P0 and P3 pups, as determined by an unpaired *t*-test (data passed the Shapiro-Wilk normality test) (Supplementary Fig. 1). In brief, retinas were dissected in Neurobasal-A medium (Gibco, Cat # 10,888,022; Grand Island, NY, USA), and cell dissociation was performed using a papain dissociation system (Worthington Biochemical Corp., Cat # LK003150; Lakewood, NJ, USA) according to the manufacturer's instructions. Retinas were dissociated in the pre-warmed papain solution at 37 °C for 5 min, after which an equal volume of inhibitor solution was added to terminate the papain digestion. Cells were spun down at 300 relative centrifugal force (RCF) for 10 min, re-suspended in 500 µL of rinsing solution (Cat # 130–091–222), and incubated with 30 µL of CD90.2 magnetic microbeads (Cat # 130–121–278) for 15 min at 4 °C. The cell suspension was then loaded into pre-wet columns (Cat # 130–042–201) with 30 µm pre-separation filters (Cat # 130–041–407) and washed 3 times with rinsing solution. All items for cell separation were purchased from Miltenyi Biotec (Bergisch Gladbach, Germany). RGCs were collected after eluting the cell suspension through a magnetic column to remove CD90.2-negative cells and seeded at a density of 125 cells/mm² in sterile 8-well chamber slides (Nunc Lab-Tek II Chamber Slide System, Cat # 154,534; Thermo Scientific; Waltham, MA, USA) that were pre-coated with poly-D-lysine (PDL, 10 µg/mL; Cat # A-003-M) and meroisin (2 µg/mL; Cat # CC085) from MilliporeSigma (Burlington, MA,

USA). The RGC culture medium contained serum-free Neurobasal-A medium supplemented with 25 μM L-glutamic acid (MilliporeSigma, Cat # G1251; Burlington, MA, USA), 2 mM L-glutamine (Cat # 35,050,061), B-27 (Cat # 17,504,044), and Penicillin-Streptomycin (Cat # 15,140,122), all purchased from Gibco (Grand Island, NY, USA). Additionally, the medium was supplemented with neurotrophic factors BDNF (50 ng/mL; Cat # 450-02) and CNTF (10 ng/mL; Cat # 450-13) from PeproTech (East Windsor, NJ, USA), as well as insulin (5 $\mu\text{g}/\text{mL}$; Cat # I9278) and forskolin (5 μM ; Cat # F3917) from Sigma-Aldrich (St. Louis, MO, USA). Embryonic stem cell-derived RGC progenitors (RGCPs) and the cultural medium were provided as a courtesy gift by Astellas Pharma US, Inc., and the cells were maintained according to the standard protocol provided by Astellas.

2.3. Retinal explant cultures

Retinal explant cultures were performed as described [42]. Briefly, mouse retinas were dissected from postnatal day 10 (P10) C57BL/6 J and B6.Cg-Tg(Thy1-YFP)16Jrs/J (Thy-1 YFP) mice (Jacksons Laboratory, stock # 003,709; Bar Harbor, ME, USA). Retina flat-mounts were cut into 6 pieces and placed with the ganglion cell layer facing onto different scaffolds that were situated in 6-well cell culture inserts (Corning, Cat # 353,090; Corning, NY, USA) and cultured in the RGC medium mentioned above. Half of the medium was replaced every 2–3 days. After 5–7 days of incubation, retinal explants were fixed and stained as described below for visualization and quantification purposes.

2.4. In vitro electrical stimulation (ES)

STG4000 stimulus generator (Multi Channel Systems; Reutlingen, Germany) was used to apply ES to primary RGCs cultured in the defined medium mentioned above. After overnight incubation, cultured RGCs received ES through platinum/iridium microelectrodes that were immersed in the culture medium and connected to the stimulus generator. A single session of biphasic ramp waveform of ES at 50 μA and 20 Hz for 15 min was delivered. Sham stimulation was delivered by immersing the microelectrodes into the culture medium without delivering electricity. Cell viability tests were performed 24 h after ES. The neurite occurrence rate and neurite lengths were quantified at 5 days of culturing post-ES, as described below.

Glutamate receptor blockers were used to investigate the relationship between ES and glutamate in RGC neurite outgrowth. The glutamate receptor blockers used in this study included: d(-)-2-amino-5-phosphonopentanoic acid (AP5, 30 μM ; Cat # A8054), (5S,10R)(+)-5-Methyl-10,11-dihydro-5H-dibenzo[a,d]cyclohept-5,10-imine hydrogen maleate (MK-801, 50 μM ; Cat # M107), 6-Cyano-7-nitroquinoxaline-2,3-dione disodium salt hydrate (CNQX, 10 μM ; Cat # C127), 1,2,3,4-Tetrahydro-6-nitro-2,3-dioxo-benzo[f]quinoxaline-7-sulfonamide disodium salt hydrate (NBQX, 10 μM ; Cat # N183), and (\pm)- α -Methyl-(4-carboxyphenyl)glycine (MCPG, 600 μM ; Cat # M196) [43,44]. All blockers were purchased from Sigma-Aldrich (St. Louis, MO, USA). Glutamate receptor blockers were added to the culture media 5 min before ES to ensure sufficient time for action (these blockers/antagonists typically begin to take effect within minutes). The blockers were present in the medium throughout the ES session and the cultural period to ensure the blockade of glutamate signaling induced during and after the ES. For quantification, 10 random images were taken from each culture well, and each experiment was repeated with 3 independent cultures.

2.5. Cell viability analysis

Cell viabilities were evaluated as described previously [36–39] using a live/dead staining kit (Invitrogen, Cat # L3224; Waltham, MA, USA), in which the green-fluorescent calcein-AM dye stains live cells by the intracellular esterase activity, while red-fluorescent ethidium

homodimer-1 (EthD-1) dye labels dead cells whose plasma membranes lose integrity. To perform the staining, culture wells were washed with phosphate buffered saline (PBS, Boston BioProducts, Cat # BM-220; Milford, MA, USA) to remove non-adhered cells. Then, 200 μL of staining solution (0.125 % calcein-AM and 0.25 % Ethd-1 in PBS) was added to each well and incubated for 30 min at room temperature (RT). After staining, cells were washed twice with PBS, and 10 random images were taken from each well immediately using a fluorescence microscope (Leica Microsystems DMI8; Wetzlar, Germany).

2.6. Immunocytochemistry staining

Immunocytochemistry staining was performed as previously reported [37,45]. Cells or retinal explants were fixed with 4 % paraformaldehyde (PFA; Electron Microscopy Sciences, Cat # 15,710; Hatfield, PA, USA) at RT for 10 min. Mouse eyeballs and optic nerves were fixed in 4 % PFA overnight at 4 $^{\circ}\text{C}$. After fixation, retinas were dissected from eyeballs for whole-mount staining. Fixed eyeballs were cryoprotected in 20 % sucrose solution, embedded in optimal cutting temperature (OCT) compound (Sakura, Cat # 4583; Torrance, CA, USA), and cryo-sectioned into 10 μm -thick slices. Specimens were rinsed with PBS before immunocytochemistry. Retinal sections and fixed cells were blocked with the blocking buffer of PBS containing 0.3 % Triton X-100 (Cat # T8787) and 1 % bovine serum albumin (BSA; Cat # A7030) from MilliporeSigma (Burlington, MA, USA), while retinas and retinal explants were blocked with PBS containing 1 % Triton X-100 and 5 % BSA solution for 30 min at RT. Primary antibodies against mouse β -III tubulin (1:400; Cat # MAB5564) or Brn3a (1:500; Cat # MAB1585) from MilliporeSigma (Burlington, MA, USA) were incubated with the blocking buffer at 4 $^{\circ}\text{C}$ overnight. Specimens were washed with PBS and incubated with Cy3- or Cy2-conjugated anti-mouse secondary antibody (1:500; Cat # 715-165-150 and 711-225-152) from Jackson ImmunoResearch (West Grove, PA, USA) in a blocking buffer at RT for 2 h. After washing, specimens were mounted with a mounting medium containing 4',6-diamidino-2-phenylindole dihydrochloride (DAPI; Abcam, Cat # ab104139; Waltham, MA, USA) and sealed with coverslips by clear nail polish. Finally, samples were visualized under a fluorescence or confocal microscope (Leica Microsystems TCS SP5, Wetzlar, Germany). The number and length of neurites were quantified and analyzed using Fiji/ImageJ software to show as results.

2.7. Scanning electron microscopy imaging

The ultrastructure of various electrospun scaffolds, 3D conduits, and cell morphologies on PBG scaffolds were visualized using scanning electron microscopy (SEM). For cell morphology, specimens were washed twice with PBS, fixed with 4 % PFA for 2 days at 4 $^{\circ}\text{C}$, and then transferred to $\frac{1}{2}$ strength Karnovsky's fixative. The specimens were subsequently dehydrated, dried, and observed under the SEM.

2.8. Scaffold preparation, evaluation, and glutamate release assessments

Polycaprolactone (PCL, Mw: 280 kDa, PDI: 1.3) was purchased from Sigma Aldrich (Cat # 440,752; St. Louis, MO, USA), and poly- γ -benzyl-L-glutamate (PBG) polymer (Mw: 200–300 kDa, PDI: 1.2–1.3) was synthesized using ring-opening polymerization method (Supplementary Fig. 2). Both materials were then fabricated into fibrous scaffolds by electrospinning as previously reported [34,35]. In brief, a high voltage was applied to the needle tip of a syringe containing the polymer solution. When the charge on the surface of the drop became sufficient, the polymer jet was pulled out and deposited on the collector to form fibrous scaffold sheets. Two fiber alignments, isotropic and aligned scaffolds, were designed. Isotropic scaffolds were prepared on the stationary metal collector, while aligned scaffolds were prepared on a rotating drum metal collector.

Fibrous sheets of the PCL and PBG were vacuum-dried overnight

before water contact angle and thickness measurements. Isotropic or aligned PBG scaffolds were incubated in PBS at 37 °C with 5 % CO₂ for the degradation and pH tests, as previously reported [34]. The weight change of the scaffolds and the pH value of the solution were measured every 7 days for up to 42 days. The glutamate concentration was measured using a glutamate assay kit (Sigma-Aldrich, Cat # MAK004; St. Louis, MO, USA) according to the manufacturer's instructions. The assay was conducted on days 0, 7, 14, and 28 to assess the concentration of glutamate released from isotropic or aligned PBG scaffolds in PBS solution at 37 °C with 5 % CO₂. Sterilized O-rings were used to ensure the scaffolds were fully immersed in the solution during incubation.

Scaffolds were cut into 7–8 mm circular specimens, detached from aluminum foil sheets, and placed into 48-well cell culture plates. All scaffolds were sterilized in the culture plates by ultraviolet (UV) light irradiation for 30 min before use. Coating substrates of PDL, PDL combined laminin/merosin, and Matrigel are all commonly used for primary RGC cultures [36–41]. We noted that while all three coatings supported RGC survival and neurite outgrowth. PDL plus merosin promoted significantly higher RGC survival and longer neurite lengths than PDL alone, while Matrigel performed the best in promoting longer neurite lengths (Supplementary Fig. 3). To ensure optimal cell adhesion and create a more physiologically relevant environment that mimics *in vivo* conditions [46,47] and maximizes neurite/nerve growth, Matrigel (10 mg/mL; Corning, Cat # 356,230; Corning, NY, USA) was used for coating the scaffolds in both *in vitro* and *in vivo* according to the manufacturer's protocol.

2.9. Constructing 3D conduits for *in vivo* transplantation

Since PBG and its hydrolyzed derivatives poly(benzyl glutamate)- γ -poly(glutamic acid) (PBG- γ -PGA) do not perform proper rheological behavior for Fused Deposition Modeling (FDM) 3D printing, we fabricated 3D printed conduits by using PCL as the base structure. The architectural design of PCL conduits was conducted using SketchUp Make 2017 (Trimble Inc.; Sunnyvale, CA, USA). The STL file of the PCL conduit was sliced by Ultimaker Cura 3.3.0 software (Ultimaker B.V.; Utrecht, The Netherlands) to generate the g-code for 3D printing. The settings of line width, layer height, brim width, and print speed were set at 200 μ m, 100 μ m, 3 mm, and 15 mm/min, respectively. During printing, the temperature of the build plate and the nozzle were set at 30 °C and 180 °C, respectively.

The Ultimaker 2 Plus 3D printer (Ultimaker B.V.; Utrecht, The Netherlands) equipped with a 250 μ m copper nozzle and a PCL filament (Facilan™ PCL 100 Filament) of 2.85 mm diameter was utilized to conduct 3D printing. After printing and removing the brim, PCL conduits were obtained. An elongated PCL (E-PCL) conduit was produced by stretching the PCL conduit to ~500 % of its original length. Following the construction of the PCL and E-PCL conduits, the inner walls were coated with 1 wt.% PBG/tetrahydrofuran (THF) solution and vacuumed dry at RT. All 3D conduits were sterilized, coated with Matrigel as described above, and cut into 1 mm size for optic nerve transplantation.

2.10. Optic nerve transection and anterograde labeling of axons

Optic nerve transection (ONT) injury was carried out as previously reported [45]. Adult C57BL/6 J mice were anesthetized with a ketamine (12.5 mg/mL) and xylazine (2.5 mg/mL) mixture (0.1 mL/20 g). The left optic nerve was exposed infraorbital. To access the optic nerve, the dura of the optic nerve was opened using a 30 G needle, followed by optic nerve transection at about 1 mm from the posterior pole of the eyeball without damaging the ophthalmic artery running along the inferior dura. A 3D-printed PBG-coated conduit was inserted into the transected site (Supplementary Fig. 4). Two weeks later, an anterograde axon tracer, cholera toxin B subunit (List Biological Laboratories, Cat # 104; Campbell, CA, USA), was injected into the vitreous cavity 3 days before euthanizing to label optic nerve fibers. After sacrifice, eyeballs with

optic nerves were collected, preserved in 4 % PFA overnight, cryo-protected with 20 % sucrose, and cryo-sectioned at 10 μ m thickness. Nerve sections were immunolabeled for cholera toxin B and imaged under the fluorescence microscope.

2.11. Statistical analysis

All data were derived from at least 3 independent experiments. Statistical analyses were conducted using the software GraphPad Prism (v. 8.3). The normality of data was examined by the Shapiro-Wilk test. If the data passed the normality test ($\alpha = 0.05$), an unpaired *t*-test or one-way analysis of variance (ANOVA) was performed, followed by a post-hoc test to compare among groups. For data that did not follow a Gaussian distribution, non-parametric ANOVA (Kruskal-Wallis test) was used to investigate the relationship between parameters. Statistical significance was determined at a *p*-value of < 0.05. Significance levels are denoted * as *p* < 0.05, ** as *p* < 0.01, *** as *p* < 0.001, and **** as *p* < 0.0001. Results are presented as mean \pm standard error of the mean (SEM) unless otherwise specified.

3. Results

3.1. ES promotes neurite outgrowth in RGCs through glutamate signaling

To investigate the effect and underlying signaling events of whether ES improves RGC neurite outgrowth [48–50] *in vitro*, a single session of 50 μ A, 20 Hz biphasic ramp ES was applied to primary RGC cultures for 15 min. We demonstrated previously that mouse RGCs exhibit dramatic loss of their intrinsic ability to regenerate axons a day before birth [42]. To assess particularly the ability of ES to promote RGC axon regeneration in the postnatal stage, we used RGCs isolated from P0–P3 mouse pups. Cultured primary mouse RGCs, which were isolated following optic nerve transection and papain dissociation, mirror the survival and axon regeneration following acute axotomy damage *in vivo*. After 5 days in culture, a significantly higher percentage of cells bearing neurites and longer neurite lengths were noted in the ES-treated group compared to controls (Fig. 1). Stimulation with low current electricity enhanced the neurite outgrowth, resulting in longer and more complex neurites (Fig. 1A), without affecting RGCs survival (Supplementary Fig. 5A). Specifically, ES led to a 1.5-fold increase in the neurite occurrence rate (Fig. 1B), a 2.5-fold longer average neurite length (Fig. 1C), or a 4-fold higher in the longest neurite length (Fig. 1D) compared to control.

We tested whether the effects of ES involve glutamate signaling since it is known to play a crucial role in supporting neurite growth during development [20,21]. To this end, we used several glutamate receptor blockers, including AP5, a competitive antagonist for N-methyl-D-aspartate (NMDA) receptors; MK-801, a selective non-competitive antagonist that blocks the ion channel of NMDA receptors; CNQX and NBQX, both selected as competitive glutamate receptor antagonists targeting α -amino-3-hydroxy-5-methyl-4-isoxazolepropionic acid (AMPA)/kainate receptors; and MCPG, a competitive antagonist against Group I (mGluR1 and mGluR5) and Group II (mGluR2 and mGluR3) metabotropic glutamate receptors. As reported, the neurite growth-inhibitory effect of glutamate antagonists is fully reversible [51–53].

As ES extensively increased RGC neurite outgrowth, the addition of any glutamate receptor blockers, including AP5, MK-801, CNQX, NBQX, and MCPG, significantly diminished the effects of ES on RGC neurite outgrowth (Fig. 1) without significantly altering RGC survival (Supplementary Fig. 5A). In particular, the presence of these glutamate receptor antagonists reduced the neurite occurrence rate by 35–50 % and decreased both the average and longest neurite lengths by 60–90 % in ES-treated cultures, bringing these measurements to or below the levels observed in the non-ES-treated control group (Fig. 1B–D). These results indicate that glutamate signaling plays a critical role in supporting ES-induced neurite outgrowth in RGCs.

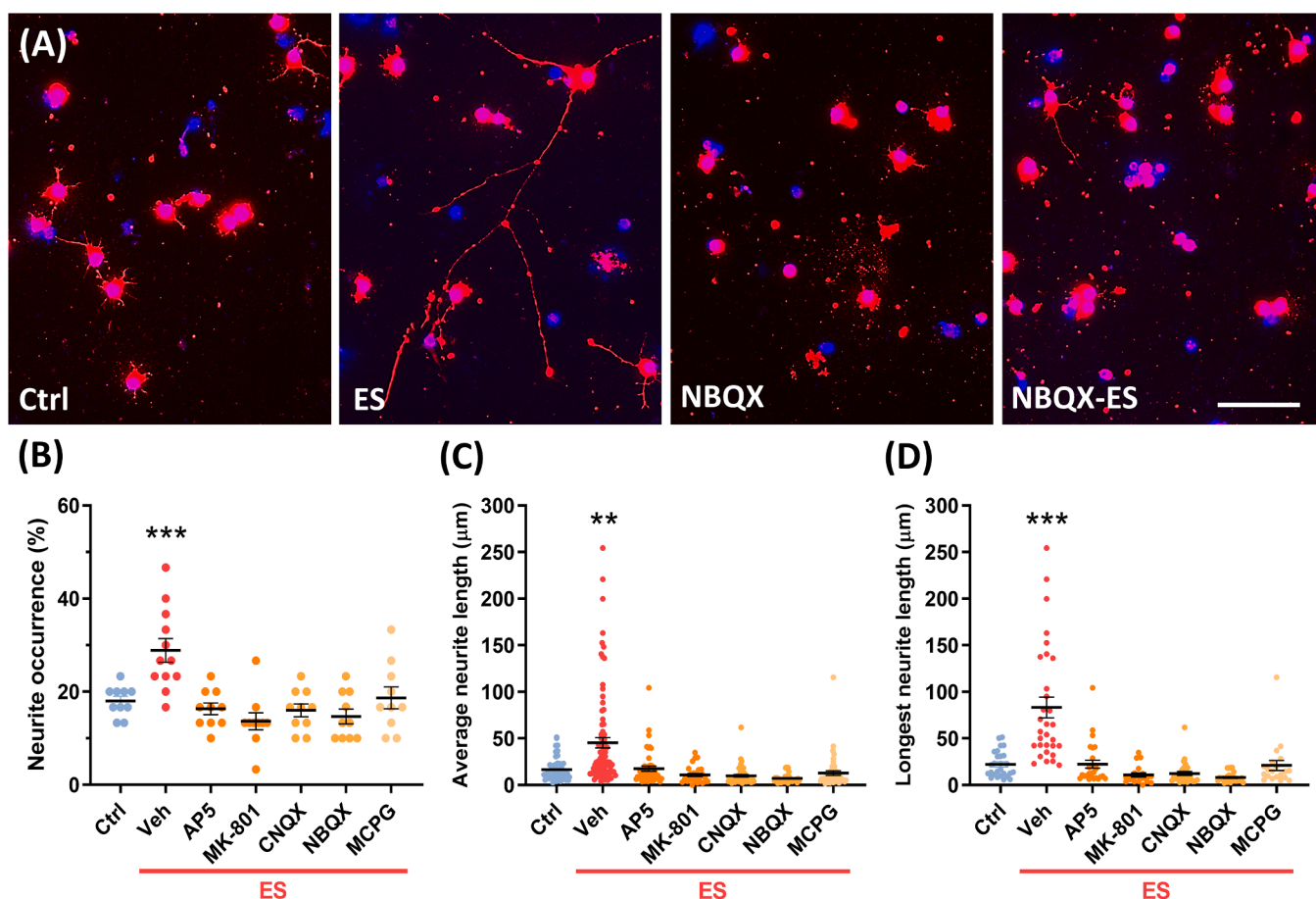


Fig. 1. Electrical stimulation promotes neurite outgrowth of retinal ganglion cells through glutamate. (A) Representative morphologies of primary RGCs, RGCs applied with ES, RGCs treated with glutamate antagonist NBQX, and RGCs pretreated with NBQX followed by ES. Red: β -III tubulin; Blue: DAPI. Scale bar = 50 μm . Quantification of (B) neurite occurrence rate, (C) average neurite length from all neurites, and (D) the longest neurite length of primary RGCs pretreated with various glutamate blockers targeting different glutamate receptors and subjected to ES. Data are presented as mean \pm SEM, $n = 10$ –12. One-way ANOVA with Dunnett's multiple comparisons test was performed for neurite occurrence analyses, while Kruskal-Wallis tests followed by Dunn's multiple comparisons were applied for neurite length analyses. ** $p < 0.01$; *** $p < 0.001$.

3.2. Designing glutamate-slow-release fibrous scaffolds

The finding prompted us to develop a polymer containing glutamate, poly- γ -benzyl-L-glutamate (PBG), which mimics the sustained ES-induced glutamate signaling to stimulate RGC neurite outgrowth. PBG was synthesized via a conventional ring-opening polymerization reaction (Supplementary Fig. 2B). A widely used FDA-approved polymer, polycaprolactone (PCL), was selected as a comparative control [54,55]. Both materials were fabricated into fibrous scaffolds by electrospinning with either isotropic or aligned fiber alignments. As shown by scanning electron microscopy (SEM), the biomimetic electrospun scaffolds of PCL and PBG featured uniform fibrous structures and 3D porous networks with isotropic or aligned fibers (Fig. 2A). Both the isotropic and aligned fibrous PCL and PBG scaffolds demonstrated similar hydrophilicity, as measured by water contact angle analysis, and had comparable thickness (Fig. 2B and C).

We also evaluated the pH level, degradability, and glutamate release kinetic of isotropic or aligned PBG scaffolds in PBS, incubated at 37 $^{\circ}\text{C}$ with 5% CO_2 over time. We noted a decrease in pH from 7.1 ± 0.1 to 6.0 ± 0.1 during the first 7 days of incubation, after which the pH remained stable between 6.5 and 6.6 for up to 42 days (Fig. 2D). As pH change may have a critical impact on cell survival and growth, we also monitored pH value changes in RGC culture medium. Remarkably, we observed a steady pH value maintained constantly between 7.7 and 7.9 over the entire period of 42 days of incubation in the RGC culture media

(Supplementary Fig. 6A), suggesting a stronger buffering capacity of the culture medium than PBS. To further determine if the pH change shown above in the PBS was a result of PBG degradation or acidification from CO_2 dissolution, we monitored the pH levels in both the PBS solution and RGC medium over time in the absence of PBG scaffolds. Results showed that the RGC medium maintained a stable pH between 7.7 and 7.9, whereas the pH level in PBS decreased from 7.1 to 6.5 over the first 2 weeks of incubation (Supplementary Fig. 6B). Therefore, the presence or degradation of PBG scaffolds did not cause significant acidity to the environment. Similar to PCL [56–58], slow degradation of the PBG scaffolds was notable following incubation from days 7–42. Isotropic PBG scaffolds (I-PBG) exhibited a higher degradation rate than aligned scaffolds, with $\sim 10\%$ mass loss compared to $\sim 5\%$ loss in aligned scaffolds by day 42, likely due to their higher exposure surface area (Fig. 2E).

In order to understand how much glutamate was being released by PBG scaffolds over time, we then evaluated the glutamate release from PBG scaffolds in culture using the glutamate assay kit. Glutamate concentrations were measured at days 0, 7, 14, and 28 to illustrate the glutamate release kinetics. Over the first 2 weeks, we observed a gradual slow glutamate release from both aligned and isotropic PBG scaffolds, with concentrations reaching 0.45 – $0.7 \mu\text{M}$ by 1 week and $3.0 \mu\text{M}$ by 2 weeks of incubation (Fig. 2F). After this point, the glutamate concentration remained unchanged through the 4th week. Given that the standard culture media for RGC neurite outgrowth assays require a

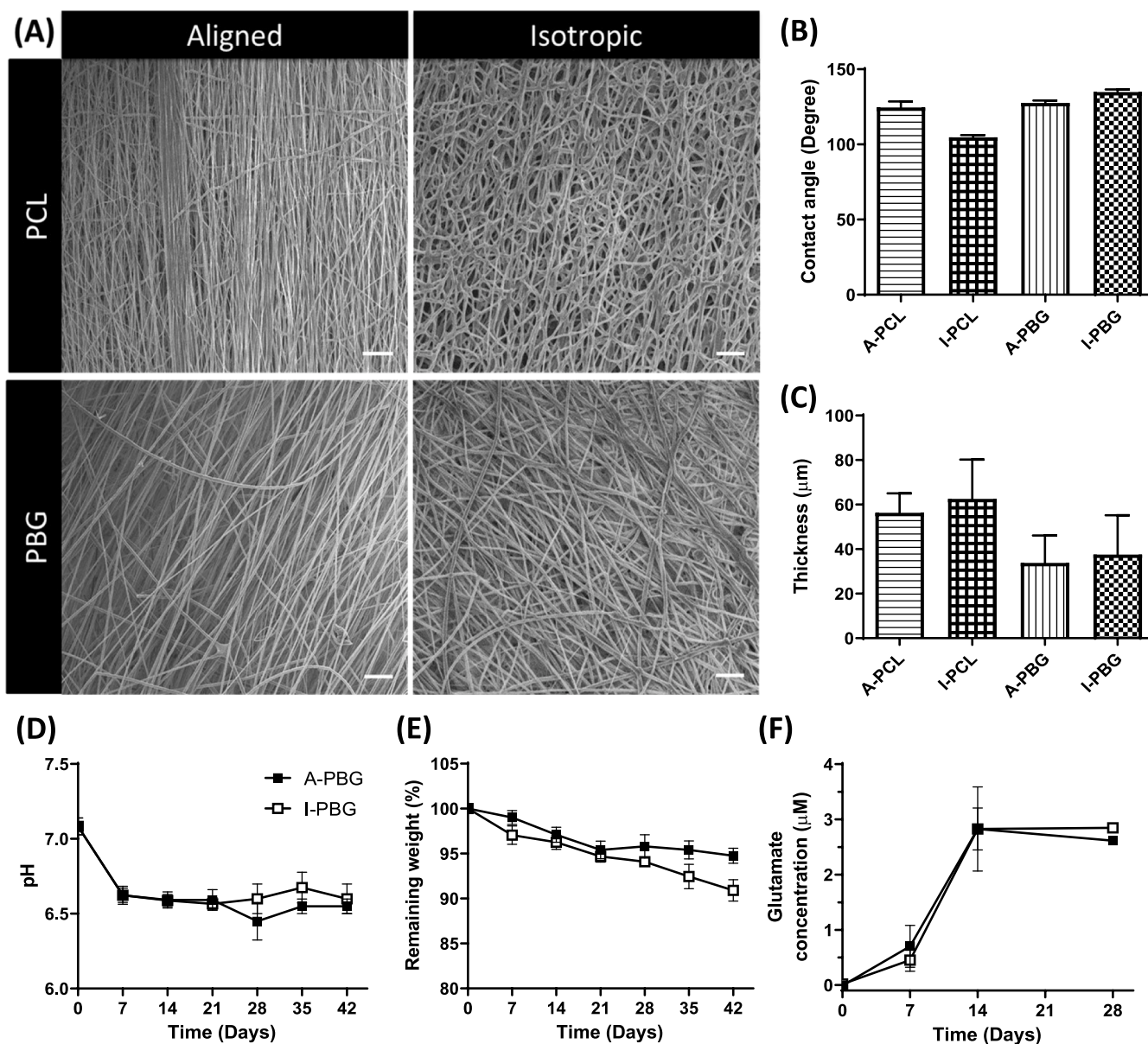


Fig. 2. Design and characteristics of the electrospun polymer scaffolds of polycaprolactone (PCL) and poly(γ -benzyl-L-glutamate) (PBG) with aligned or isotropic fiber alignment. (A) Representative scanning electron micrographs of aligned and isotropic scaffolds of PCL and PBG (500X). Scale bar = 20 μm . (B) Contact angles and (C) thicknesses of the fabricated scaffolds. Data are presented as mean \pm SD, $n = 3/\text{group}$. (D) pH levels and (E) degradation rates of aligned PBG (A-PBG, black square) and isotropic PBG (I-PBG, white square) scaffolds incubated in PBS solution at 37 $^{\circ}\text{C}$ with 5% CO_2 over 42 days. Data are shown as mean \pm SEM, $n = 3 - 7/\text{group}$. (F) Glutamate concentrations released from PBG scaffolds in PBS solution over a 28-day incubation period. Data are shown as mean \pm SEM, $n = 6/\text{group}$.

supplement of 12.5 – 25 μM glutamate for optimal neuronal survival [36–39], the free-glutamate released from PBG scaffolds should have minimal impact on RGC survival and neurite growth. Direct contact of RGC neurites with PBG-bound glutamate is likely to play a more important role in driving their axon extension.

In summary, both isotropic and aligned PCL and PBG scaffolds demonstrated similar physical properties. The slow degradability and sustained release of low concentrations of glutamate from the PBG scaffold make it an ideal biomaterial for supporting nerve regeneration after injury. It provides mechanical bridging support and continuous glutamate stimulation, which could potentially facilitate nerve regeneration and be gradually replaced by natural extracellular matrix (ECM) networks upon completion of the regeneration process.

3.3. PBG scaffolds promote RGC survival and neurite outgrowth in culture through glutamate signaling

We sought to investigate if PBG scaffolds improve RGC survival and promote the ability of neurite outgrowth in culture. Primary mouse RGCs were cultured on cover glass (CG), PCL, or PBG that had been pre-coated with Matrigel for 1–5 days. We found that RGCs grown on PBG scaffolds exhibited significantly increased survival and neurite outgrowth compared to the CG and PCL groups (Fig. 3A–C). There was a 3-fold increase in the percentage of surviving RGCs in the PBG scaffold group than the PCL scaffold and CG groups when assessed after 1 day of culturing (Fig. 3A). Moreover, there were over 2-fold increases in the neurite occurrence rate as well as the longest neurite lengths in PBG scaffold group comparing to PCL controls following 5 days of culturing (Fig. 3B and C). Cultured RGCs extended long neurites along the direction of PBG fibers (Fig. 3D and E). Many fine neurites were also

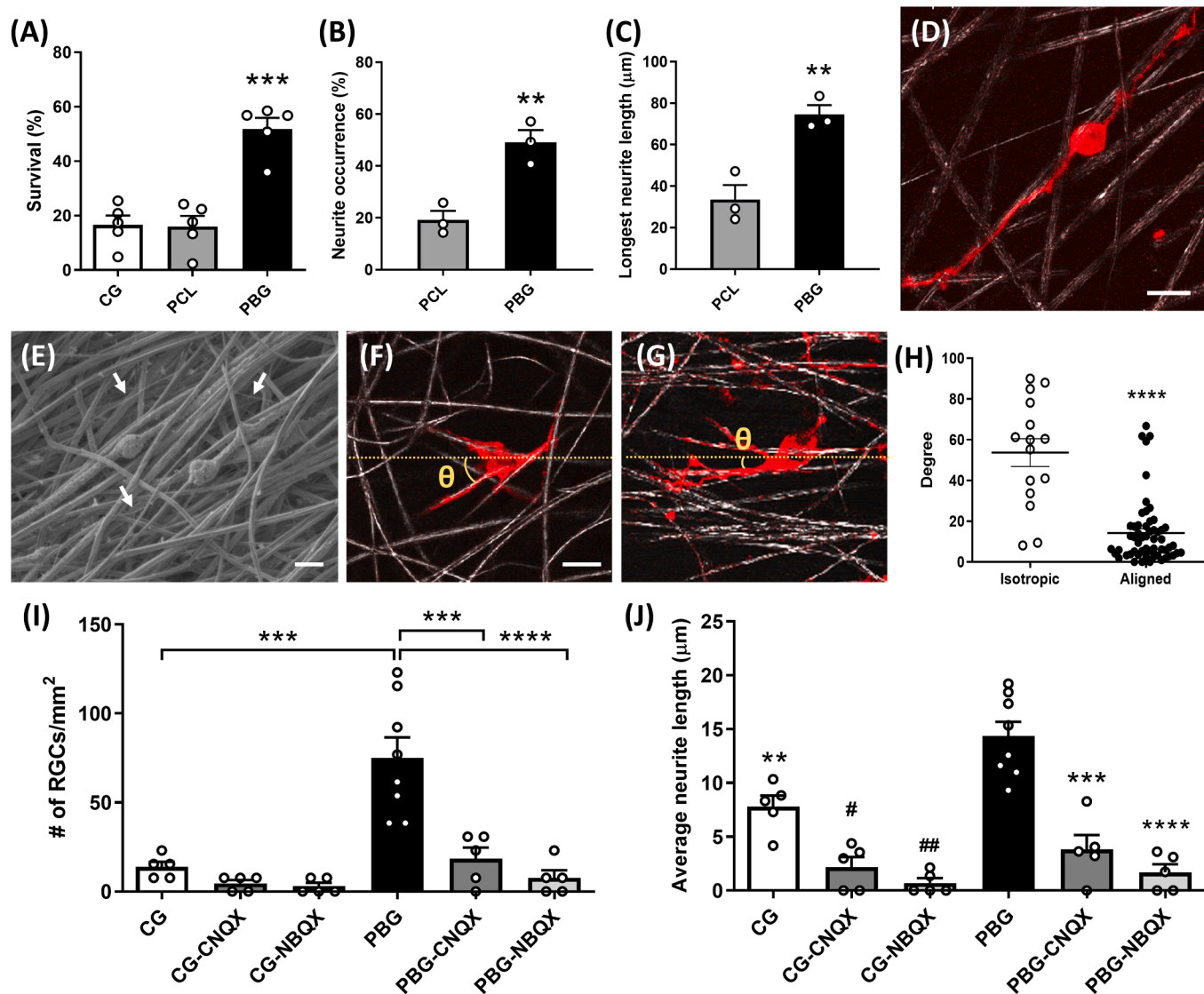


Fig. 3. PBG scaffolds support survival and stimulate neurite growth of primary retinal ganglion cells (RGCs) through glutamate signaling. (A) Survival rates of primary mouse RGCs growing on cover glass (CG), PCL, and PBG scaffolds, respectively. $n = 5$. (B) Neurite occurrence rate, and (C) longest neurite length of RGCs cultured 5 days on PCL and PBG scaffolds. $n = 3$. (D) Representative image of single RGC nerve processes growing along the fiber of the PBG scaffold, showing long extended neurites. Gray: Scaffold fibers; Red: β -III tubulin. Scale bar = 10 μm . (E) Representative scanning electron microscopy (SEM) image illustrating the ultrastructure of RGCs growing on the surface of PBG scaffold with fine neurites interconnecting the PBG fibers (arrows). Scale bar = 10 μm . Representative confocal images of measuring the angle of RGC neurites growing on an (F) isotropic PBG scaffold and (G) aligned PBG scaffold. Gray: Scaffold fibers; Red: β -III tubulin. Scale bars = 20 μm . (H) Angle distribution of RGC neurites growing on isotropic versus aligned PBG scaffolds. (I) Number of RGCs with neurite outgrowth longer than the cell body and (J) average neurite length of RGCs growing on CG and PBG scaffolds with or without AMPA/kainate glutamate receptor antagonists after 3 days of culture. *Compared to PBG; # compared to CG. $n = 5$ –8. Data are shown as mean \pm SEM. One-way ANOVA with Tukey's multiple comparisons test was performed for plots (A, I, J); unpaired t -tests were applied for plots (B, C, H). * $p < 0.05$, ** $p < 0.01$; *** $p < 0.001$; **** $p < 0.0001$.

observed wrapping around the fibers of the PBG scaffold under ultrastructure (Fig. 3E), demonstrating the biocompatibility of the material. We further analyzed the angles of neurites growing on isotropic or aligned PBG scaffolds (Fig. 3F and G). Results showed that RGC neurites distributed in all directions on isotropic scaffolds by following a random orientation of PBG fibers. In contrast, neurites on aligned PBG scaffolds closely followed the fiber alignment, growing within 15° or less with the aligned fibers (Fig. 3H).

To verify that PBG scaffolds promote neurite outgrowth of RGCs through glutamate signaling, glutamate receptor antagonists CNQX and NBQX were added to the culture medium. CNQX and NBQX were selected due to being the most effective antagonists in blocking the ES-induced RGC neurite growth (Fig. 1B–D). The results showed that when RGCs were cultured on PBG scaffolds, the number of RGCs with neurites

longer than the cell body length increased more than 5-fold compared to those growing on a CG surface when measured at 3 days of incubation. The addition of CNQX and NBQX drastically reduced the number of neurite-bearing RGCs on PBG scaffolds ($p < 0.001$) (Fig. 3I). Similar findings were observed when the average neurite length was quantified. The neurites of RGCs growing on PBG scaffolds extended twice as long as those on CG, while the administration of CNQX and NBQX significantly attenuated the growth-promoting effects of PBG scaffolds, resulting in neurite lengths even shorter than those in the CG control group (Fig. 3J). Furthermore, CNQX and NBQX also significantly reduced RGC neurite lengths in the CG control group, suggesting that endogenous glutamate signaling is involved in normal RGC neurite extension. (Fig. 3J and Supplementary Fig. 5B–D). The reduction was found more pronounced with AMPA/kainate receptor antagonists, implying that AMPA/kainate

receptors may play a more critical role in maintaining neurite outgrowth. Together, these findings indicate that PBG scaffolds support cell survival, neurite outgrowth, and direct neurite extension through glutamate signaling.

3.4. PBG scaffolds promoted robust neurite outgrowth from retinal explants

To investigate if PBG scaffolds promoted nerve regeneration and regrowth from damaged retinal tissues, mouse retina explants were dissected and cultured on isotropic or aligned PCL and PBG scaffolds placed on top of a permeable cell culture insert. After 5 days of incubation, neurite outgrowth from the retinal explants was visualized using β -III-tubulin immunolabeling and subsequently quantified (Fig. 4). Limited numbers of neurites were observed on either isotropic or aligned PCL scaffolds (Fig. 4A and B). The average neurite length growing on PCL scaffolds was less than 200 μm (Fig. 4C), with the longest neurites not surpassing 500 μm (Fig. 4D). In contrast, PBG scaffolds significantly promoted robust neurite outgrowth from retinal explants (Fig. 4A). More than double of the neurite numbers were counted from those growing on PBG scaffolds than on PCL controls (Fig. 4B). Moreover, PBG scaffolds supported longer neurite outgrowth, with average lengths of 500–600 μm (Fig. 4C) and the longest neurites typically reaching 1200–1300 μm (Fig. 4D). Notably, neurite outgrowth appeared more

pronounced in the aligned PBG (A-PBG) group, with longer in average and more organized neurites compared to other conditions. Many neurites found in the A-PBG group extended beyond 1500 μm in length, following the direction of PBG fibers, and developed growth cone-like structures at the terminal of extending neurites.

To further validate that PBG scaffolds promoted the growth of RGC axons, retinal explants from Thy-1 YFP mice carrying a yellow-fluorescence protein (YFP) reporter gene driven under a Thy-1 promoter, allowing direct visualization of RGC neurites through YFP expression [59]. The co-localization of β -III tubulin-positive neurites with Thy-1 YFP signals confirmed that these neurites primarily originated from RGCs. The neurites were long and healthy, growing along with the alignment of A-PBG scaffold fibers. After 7 days of culture, some neurites could extend up to 2.5 mm, nearly 1/3 of the length of the mouse optic nerve (Fig. 4E). These results indicate that aligned PBG scaffolds have significant potential to promote nerve regeneration and support nerve regrowth from damaged retinas.

3.5. PBG scaffolds provided support for neurite outgrowth of RGCs

The approach of cell therapy for replacing damaged or dying RGCs is emerging as a promising strategy for retinal degenerative diseases and/or optic neuropathy while inducing axon elongation from iPSC or ESC-derived RGC progenitors (RGCs) presents a major obstacle in its

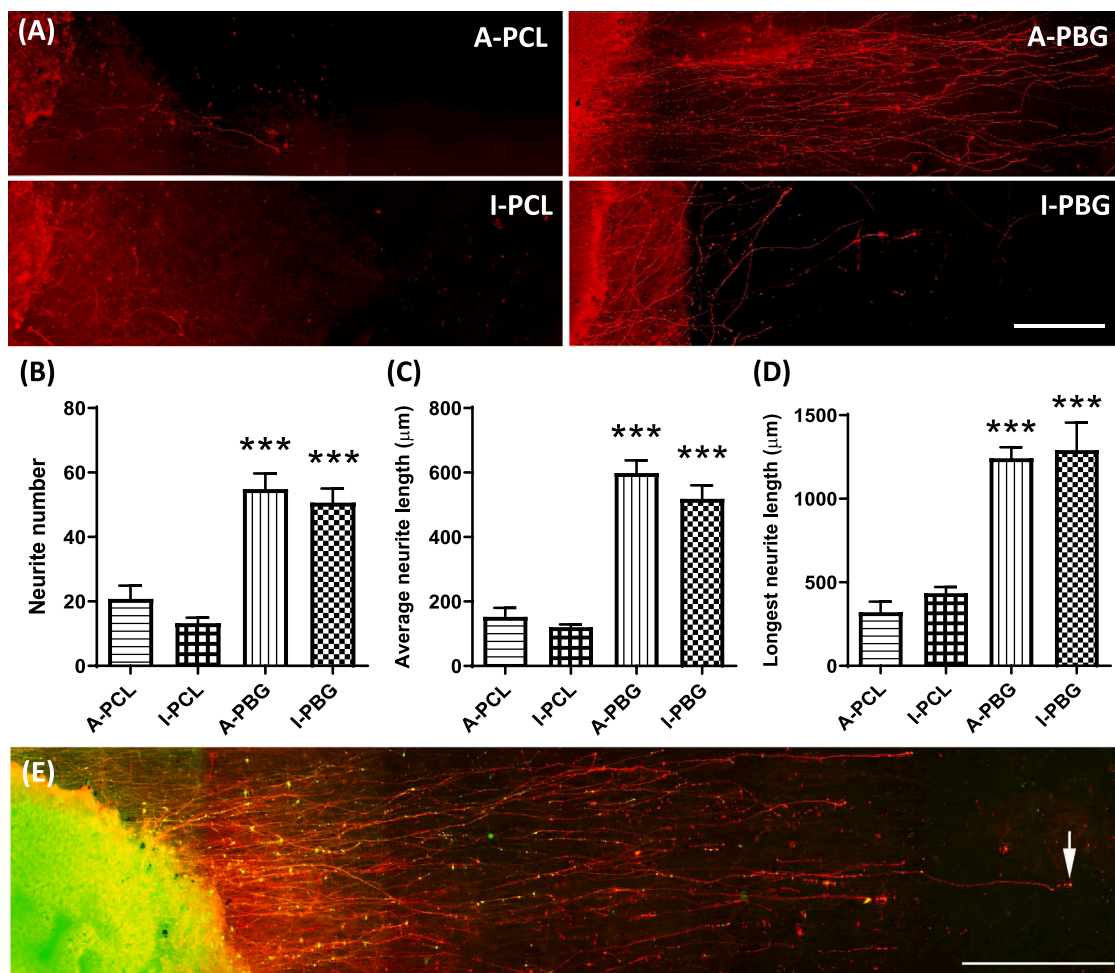


Fig. 4. Retinal explants develop long and robust neurites aligned with the direction of PBG fibers. (A) Morphology of neurite outgrowth from retinal explants cultured on aligned or isotropic PCL and PBG scaffolds. Scale bar = 250 μm . (B) Quantification of the neurite numbers per 1000 μm across different scaffolds. Quantification of (C) average neurite length and (D) longest neurite length on various scaffolds after a 5-day culture. (E) Morphology of a Thy-1 YFP positive retinal explant co-stained with β -III tubulin (red) on an aligned PBG scaffold. Arrow indicated the longest extended neurite with a growth cone-like structure. Scale bar = 500 μm . Data are shown as mean \pm SEM, $n = 3$ –5. One-way ANOVA with Tukey's multiple comparisons test was performed for the statistical analysis. *** $p < 0.001$.

applications. To address this, we evaluated whether PBG scaffolds could also support RGCP differentiation and direct their axonal growth. RGCPs were derived from ESCs following a standard protocol and showed high expression of RGCP markers, including *Math5*, *Brn3a*, and *Otx2*. After differentiating into RGC-like neurons, these cells expressed *Brn3a*, Neurofilament, and β -III tubulin with extended axons (data not shown).

Our findings demonstrated that PBG scaffolds supported the survival and promoted the neurite outgrowth of RGCPs (Fig. 5). After 24 h of culturing, a significantly higher number of RGCPs on PBG scaffolds extended neurites compared to those on PCL controls, while similar numbers of surviving cells were observed across groups. After 5 days of incubation, robust survival and extensive neurite outgrowth of PRGPs were found on PBG scaffolds. RGCPs developed highly organized and interconnected long neurites that elongated along the aligned fibers of A-PBG scaffolds, while those on I-PBG scaffolds extended in multiple directions, following the random orientation of isotropic PBG fibers. In contrast, PCL scaffolds could not support RGCP survival and neurite outgrowth for up to 5 days. Cells were fewer and less viable, with little or barely any neurites observed on either aligned or isotropic PCL scaffolds (Fig. 5A). It seemed that the mechanical structure provided by aligned scaffolds appeared to play an important role in supporting cell survival and nerve growth of neural progenitors, as cell numbers and neurite extensions were greater on both aligned scaffolds compared to their isotropic counterparts by day 5 (Fig. 5A). The neurite length of RGCPs growing on A-PBG scaffolds ranged from approximately 100 to 300 μ m, with some neurites extending up to 400 μ m and exhibiting a growth cone-like structure (Fig. 5B). From the SEM image, axons from RGCPs were found growing along with the PBG fibers with many extended fine neurites wrapping around the surrounding scaffold (Fig. 5C). This observation may explain why PBG scaffolds maintained better cell adherence and growth. With the mechanical support and the neuronal

stimulatory cue of glutamate, aligned PBG scaffolds could serve as an ideal biomaterial for supporting cell survival and directing axon growth in optic nerve regeneration.

3.6. PBG-coated 3D conduits promoted optic nerve repair and regeneration

To assess whether PBG scaffolds could promote optic nerve repair and regeneration *in vivo*, we designed a proof-of-concept study by constructing a 3D-printed conduit for nerve transplantation in adult C57BL/6 J mice. Since PBG and its hydrolyzed derivatives PBG- γ -PGA did not perform proper rheological behavior for fused deposition modeling in 3D printing, we fabricated the 3D conduits using PCL as the base structure, followed by coating with a soluble PBG/THF solution and vacuumed dry. The hollow structure and dimensions of the 3D conduit are critical for successful transplantation, as they provide proper support for nerve regeneration and regrowth. The SEM imaging showed that our 3D-printed PCL conduits retained the designed hollow tubing structure, with inner diameters ranging from 200 to 300 μ m (Fig. 6A). The inner walls of PCL conduits featured a smooth, aligned ultrastructure (Fig. 6B), and the PBG coating was homogeneously distributed within the conduits (Fig. 6C).

To evaluate the biocompatibility *in vivo*, PBG scaffolds were cut into small pieces and injected intravitreally with saline. After 7 days, mouse retinal flat-mounts were collected and quantified for RGC survival using *Brn3a* immunolabeling. No significant differences in the number of *Brn3a*⁺ RGCs were observed and quantified between naïve and PBG-injected mice (Fig. 6D and E). Again, this demonstrated the low cytotoxicity and biocompatibility properties of the PBG biomaterial.

Finally, the optic nerve of adult mice was transected unilaterally by a microscissor, and a \sim 1 mm length of PBG-coated 3D conduit was placed

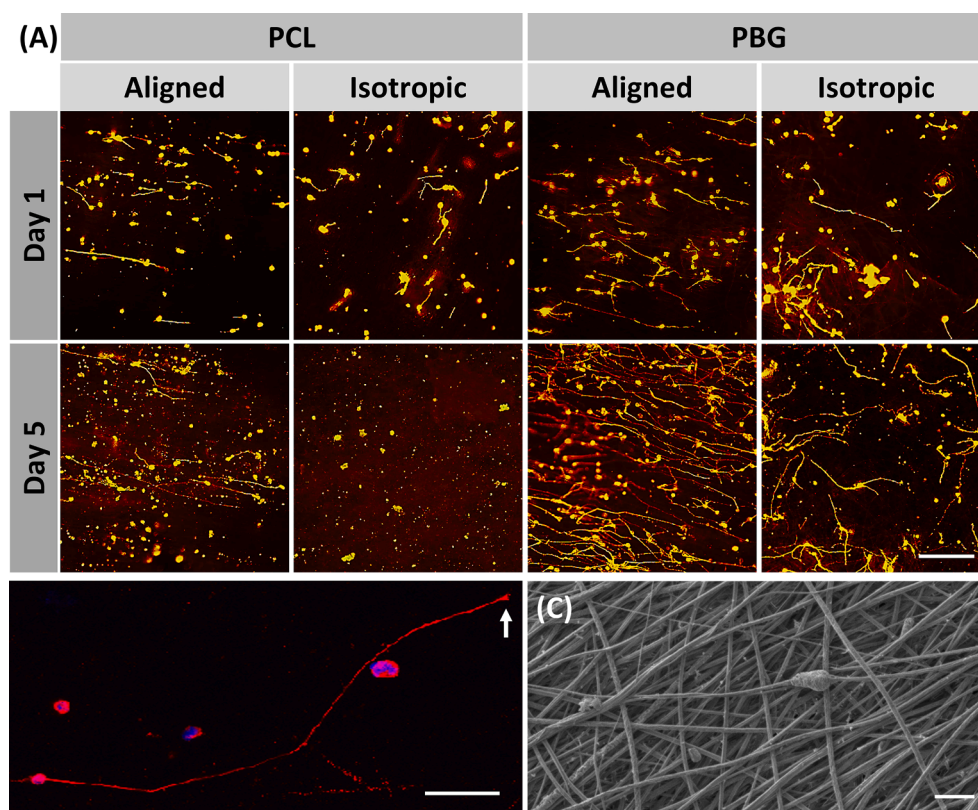


Fig. 5. Retinal ganglion cell progenitors (RGCPs) exhibit long and robust neurite growth on PBG scaffolds. (A) Morphology of RGCPs on aligned or isotropic fibers of PCL or PBG scaffolds after 1-day and 5-day culture periods. Yellow: β -III tubulin. Scale bar = 100 μ m. (B) Representative image of an RGCP extending a long neurite with a growth cone-like structure (arrow) on a PBG scaffold. Red: β -III tubulin; Blue: DAPI. Scale bar = 50 μ m. (C) Representative SEM image showing RGCPs growing along PBG fibers, with numerous fine neurites wrapping around the fibers. Scale bar = 20 μ m.

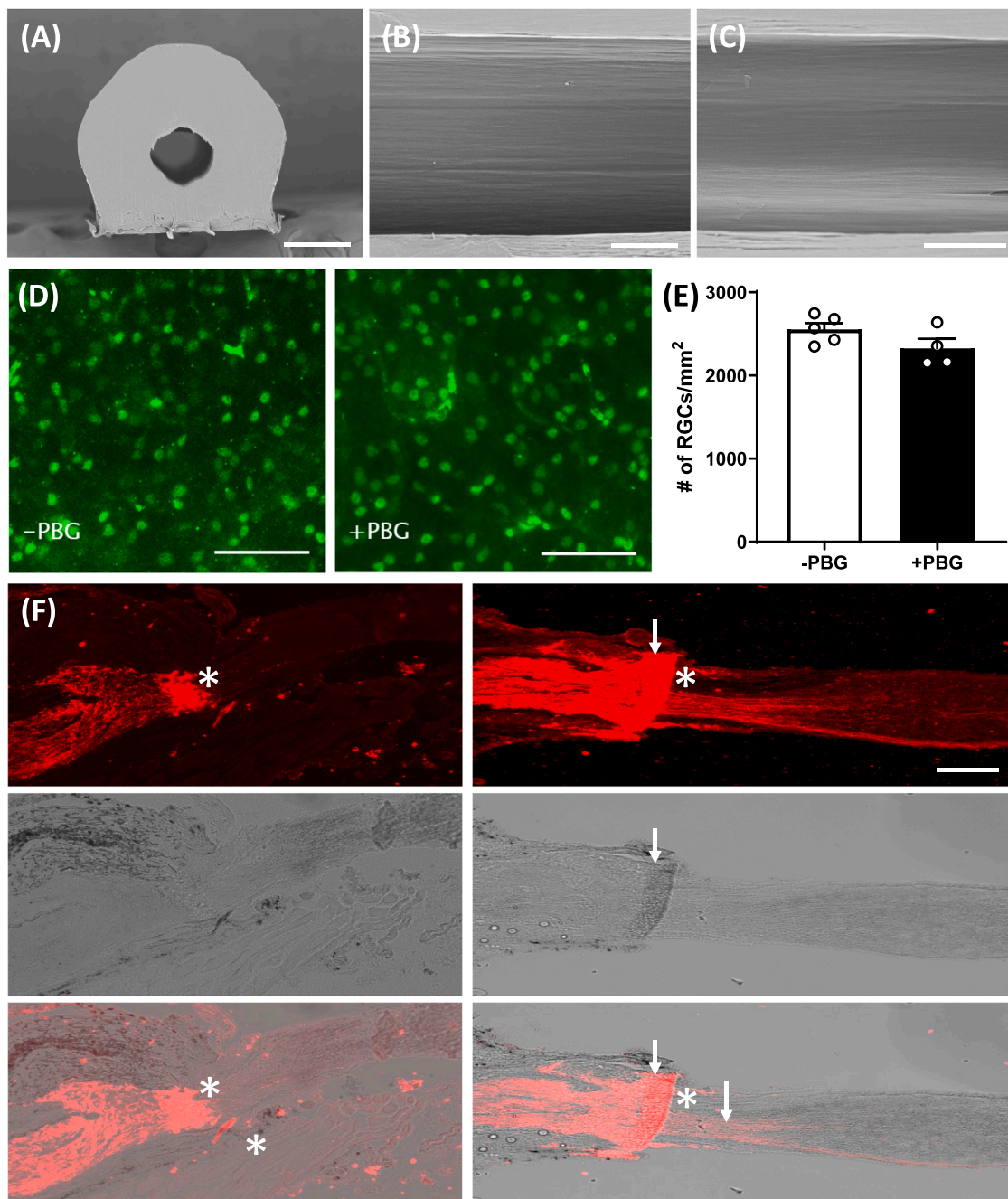


Fig. 6. PBG-coated 3D conduit exhibits the potential for optic nerve repair and regeneration. (A) Representative SEM image of the cross-section of a 3D-printed PCL conduit. The 3D conduits maintained the hollow tubing structure as designed. Scale bars = 300 μ m. Representative SEM images of the inner wall of (B) a 3D-printed PCL conduit and (C) a PCL conduit after PBG coating. Scale bars = 100 μ m. (D) Representative RGC distributions in the retinal flat-mounts of Naïve (left panel) or PBG-injected (right panel) mice after 7 days. (E) Quantification of RGC densities with or without PBG injection in the retinal flat mounts. (F) Photomicrographs of CTB-immunolabeled optic nerve fibers (top panel), phase-contrast images of optic nerve tissue sections (middle panel), and merged images of CTB-labeling and optic nerve tissue section (bottom panel) taken from mice received control (left panel) or PBG-coated 3D conduit (right panel) after optic nerve transection. Arrow indicates the transplanted conduit location. Asterisk denotes the position posterior to the nerve transection site. Scale bar = 200 μ m. Scale bar = 200 μ m. Data are shown as mean \pm SEM, $n = 5$. Unpaired t -tests.

immediately between two cutting ends of the nerve to bridge the gap (Supplementary Fig. 4). Mice without receiving a conduit served as controls. Eleven days after optic nerve transection (ONT), an anterograde axon tracer, cholera toxin B subunit (CTB) conjugated with Rhodamine, was injected intravitreally to label RGC axons. Remarkably, robust axon regeneration was observed in mice that received the PBG-coated 3D conduit, with CTB-labeled regenerating axons extending up to 1.2 mm posterior to the transection site. In contrast, only a few CTB-positive axons were detected passing the transection site in the control

group (Fig. 6F). Additionally, we have quantified the density of RGCs from retinal sections of mice with or without 3D conduit transplantation after ONT and compared them to naïve animals. Quantitative analysis revealed that the group transplanted with PBG-coated 3D conduits had a higher number of surviving RGCs than those without. RGC density was maintained at a level similar to that of naïve animals, while a significant decrease in RGC numbers was observed in the group without conduit transplantation following ONT (Supplementary Fig. 7).

Our findings indicated that the PBG-coated conduit not only could

promote axon regeneration but also protected RGCs from apoptosis after nerve transection without inducing excitotoxicity to the damaged site. On the contrary, the 3D conduit seemed to protect RGCs from apoptosis. These results suggest that PBG-coated 3D conduits present a promising strategy for promoting optic nerve repair and regeneration.

4. Discussion

While cell therapy opens a wide therapeutic window for retinal degeneration, it remains challenging due to the limited ability of transplanted RGCs to survive, integrate into the host retina, and extend long neurites through the optic nerve rewiring the visual circuit. It has been known that an appropriate scaffold made of bioactive materials with 3D structures can mimic the microenvironment of the regeneration site [60]. Therefore, constructing a biocompatible scaffold that can direct axonal growth towards the optic nerve head that can eventually reach targets in the brain may further enable cell replacement as a potential therapy for retinal degeneration diseases or optic nerve injuries in the future.

While the neuroprotective strategy of ES provided benefits to retinal neurons in animal studies and clinics, the optimal stimulation parameters have not been established for each cell type or specific retinal disease. As we showed in this paper, ES promoted RGC neurite outgrowth via glutamate signaling. There is ample evidence for the role of local neurotransmitter glutamate acting on axon terminals and/or growth cones in promoting neurogenesis and nerve growth during development [18–20,61–66]. All glutamate receptors are distributed throughout the neurons, including the soma, axon terminals, and growth cones [67,68]. Thus, PBG scaffolds can potentially stimulate nerve growth and regeneration by acting on neuronal cell bodies and axon terminals.

The distribution and types of glutamate receptors can vary depending on the neuron type and its developmental stage, allowing a wide range of functions, including synaptic transmission, plasticity, and development, that are subject to regulation by activity and developmental cues. For instance, the presynaptic glutamate receptors (e.g. AMPA/kainite) on axon terminals and growth cones respond to stimulation in a concentration-dependent manner to mediate neurite outgrowth and guidance [64,69–71]. Glutamate and neurotrophic factors work closely together to regulate neural development and neuroplasticity. Glutamate can stimulate the production of several neurotrophic factors, including brain-derived neurotrophic factor (BDNF), nerve growth factor (NGF), glial cell line-derived neurotrophic factor (GDNF), insulin-like growth factor 1 (IGF-1), and basic fibroblast growth factor (bFGF) to regulate glutamate sensitivity, calcium homeostasis, and neural plasticity [18]. Increased expression of neurotrophic factors is known to support the survival of existing neurons, as well as encourage growth and differentiation in developing neurons [72, 73]. We have tested different glutamate blockers, including AP5 and MK-801, which target NMDA receptors; CNQX and NBQX, which are antagonists of AMPA receptors; MCPG as a competitive antagonist against multiple mGluRs. Results revealed that all antagonists/blockers, to some extent, decrease the neurite occurrence and lengths (**Supplementary Fig. 5B–D**), indicating that primary RGCs depend on glutamate for normal neurite growth and extension. The reduction was found to be more significant with AMPA/kainate receptor antagonists, which suggests AMPA/kainate receptors may play a more fundamental role in maintaining neurite outgrowth.

Studies have shown that biomaterials conjugated with neurotransmitters can promote the viability, adhesion, and differentiation of neurons [74]. While PBG is a type of polypeptide made of repeating units of benzyl-L-glutamate (**Supplementary Fig. 2**), it shows many advantages for tissue engineering, including the ability to self-assemble, biocompatibility, and biodegradability [34,35]. When PCL scaffolds, which provide similar mechanical properties for axon support and bridging, were used as controls, we detected significantly enhanced axon growth in the group plated on a PBG scaffold compared to controls. Moreover,

the presence of glutamate antagonists or blockers abolished the neurite growth-promoting effect of PBG, further supporting that glutamate signaling, rather than the mechanical bridging properties of PBG, is crucial for the regenerative effects.

While PBG scaffolds were designed to be degraded over time, the rate of their degradation is found to be slow. PBG scaffolds exhibited ~5–10 % loss of mass by 42 days of incubation, similar to the reported rate of PCL degradation [57,58]. If the degradation rate remains constant, complete degradation is projected to be at 15–30 months. However, it is generally believed that the degradation of biomaterials proceeds faster under normal physiological conditions than they are in culture. In all cases, it should be interesting to monitor the conduit degradation for a longer period *in vivo*. In line with the slow rate of PBG degradation, glutamate release from the PBG scaffolds was minimal; most glutamate subunits remained conjugated in the polymers. We propose that cells indeed bind to glutamate in the polymers through direct contact with the scaffold to signal neuronal survival and neurite outgrowth. In addition, scaffolds with aligned orientation are beneficial for directing neurites growing toward the same direction through contact guidance [75–77]. Contact guidance refers to the phenomenon for which the orientation of cells is influenced by geometrical patterns, such as parallel microgrooves of a substratum. It is caused by the focal adhesion of fibronectins and integrins interacting with the fiber surface, rearranging the cytoskeletons of the cells [78]. Furthermore, increased cell numbers and longer neurite lengths were found on aligned scaffolds, compared to isotropic scaffolds with the same biomaterial. Thus, providing proper structural support for directional growth is most beneficial for nerve regeneration.

The formation of glial scar presents one of the major barriers to axon regeneration after injury. Previous studies have shown that PCL conduits limit scar tissue formation in the spinal cord injury model and demonstrate biocompatibility with multiple tissue engineering applications [55,79]. Thus, our 3D-printed conduits were designed to use PCL as the base structure that was coated with PBG. As a result, we did not observe apparent scar formation around the injury site. Further studies are needed to gain a comprehensive understanding of the effect of the 3D conduit on glial cells and their activation of reactive gliosis.

In summary, we showed that PBG scaffolds, especially with aligned fibers, have great potential to assist neural differentiation and growth of neural progenitors and support neurite elongation in a highly organized manner for transplantation purposes. The aligned PBG scaffold is a promising candidate for assisting nerve repair and regrowth in optic nerve injury models. Since retinal neurons and optic nerve are considered the most accessible in the CNS, we believed that it may not only be beneficial for reconstructing the optic nerve and helping patients to restore their vision; but also use the optic nerve as a model, to study the possibilities of regeneration on the CNS with a wide range of applications for tissue engineering.

5. Conclusion

The purpose of this study is to develop a biocompatible scaffold for promoting RGC survival and optic nerve regeneration after injury. Here, we demonstrated *in vitro* that ES promotes neurite outgrowth of RGCs. Moreover, we noted that ES worked through glutamate signaling. Thus, PBG scaffolds were designed mimicking glutamate stimulation to support robust neurite outgrowth *in vitro* and optic nerve regeneration *in vivo*. In this study, we have designed, synthesized, and fabricated a polypeptide-based biomimetic 3D scaffold containing the neuronal cue of glutamates. The PBG scaffolds showed biocompatibility and could degrade hydrolytically over time, which is beneficial for tissue engineering applications. PBG scaffolds supported the survival and neurite outgrowth of primary RGCs. With the aligned features, aligned PBG scaffolds promoted robust long neurites along with the fibers towards the same direction. Offering ideal guidance through mechanical and chemical support for axon elongation and nerve regeneration.

CRediT authorship contribution statement

Karen Chang: Data curation, Formal analysis, Investigation, Methodology, Software, Validation, Visualization, Writing – original draft, Writing – review & editing, Funding acquisition, Conceptualization. **Jhih-Guang Wu:** Data curation, Formal analysis, Investigation, Methodology, Resources, Validation, Visualization. **Tien-Li Ma:** Data curation, Formal analysis, Investigation, Resources, Validation, Methodology. **Sheng-Hao Hsu:** Data curation, Formal analysis, Investigation, Methodology, Resources, Software, Validation, Visualization, Writing – original draft. **Kin-Sang Cho:** Conceptualization, Data curation, Investigation, Methodology, Resources, Supervision, Visualization, Writing – review & editing. **Zicheng Yu:** Data curation, Formal analysis, Investigation, Visualization. **Anton Lennikov:** Resources, Software, Visualization, Writing – review & editing. **Ajay Ashok:** Data curation, Validation, Visualization, Writing – review & editing. **Aishwarya Rajagopalan:** Data curation, Validation, Writing – original draft, Writing – review & editing. **Min-Huey Chen:** Funding acquisition, Resources, Supervision, Writing – review & editing. **Wei-Fang Su:** Conceptualization, Funding acquisition, Project administration, Resources, Supervision, Validation, Writing – review & editing. **Tor Paaske Utheim:** Conceptualization, Funding acquisition, Project administration, Resources, Supervision, Writing – review & editing. **Dong Feng Chen:** Conceptualization, Funding acquisition, Project administration, Resources, Supervision, Validation, Visualization, Writing – review & editing.

Declaration of competing interest

The authors declare that they have no competing interests in financial or personal relationships that could have appeared to influence the work reported in this paper.

Acknowledgment

This research was supported by grants from: The Norwegian Research Council; The Norwegian Association for the Blind and Partially Sighted; The Department of Ophthalmology and Department of Medical Biochemistry, Oslo University Hospital, Oslo, Norway; The Ministry of Science and Technology of Taiwan (MOST 105–2917-I-002–031 and MOST 109–2917-I-564–032); NIH/NEI EY031696; EY033882; Department of Defense VR220112; Core Grant for Vision Research from NIH/NEI to the Schepens Eye Research Institute (P30EY003790).

We would also like to express our gratitude to Zhen-Hua Wang, Chia-Yu Lin, Po-Ki (Mary) Chau, Yagi Makoto, Marie Kametani, and María Camila Lancheros Vega for their help with experiments in this study.

Supplementary materials

Supplementary material associated with this article can be found, in the online version, at [doi:10.1016/j.actbio.2024.10.023](https://doi.org/10.1016/j.actbio.2024.10.023).

References

- [1] GBD 2019, Blindness and vision impairment collaborators; vision loss expert group of the global burden of disease study. trends in prevalence of blindness and distance and near vision impairment over 30 years: an analysis for the global burden of disease study, *Lancet Glob. Heal.* 9 (2) (2021) e130–e143.
- [2] GBD 2019, Blindness and vision impairment collaborators; vision loss expert group of the global burden of disease study. causes of blindness and vision impairment in 2020 and trends over 30 years, and prevalence of avoidable blindness in relation to VISION 2020: the right to sight: an analysis for the global burden of disease study, *Lancet Glob. Heal.* 9 (2) (2021) e144–e160.
- [3] D.J. Calkins, M. Pekny, M.L. Cooper, L. Benowitz, Lasker/IRRF Initiative on astrocytes and glaucomatous neurodegeneration participants. the challenge of regenerative therapies for the optic nerve in glaucoma, *Exp. Eye Res.* 157 (2017) 28–33.
- [4] W. Tong, H. Meffin, D.J. Garrett, Ibbotson MR. Stimulation strategies for improving the resolution of retinal prostheses, *Front. Neurosci.* 14 (2020) 262.
- [5] A. Müller, T.G. Hauk, D. Fischer, Astrocyte-derived CNTF switches mature RGCs to a regenerative state following inflammatory stimulation, *Brain* 130 (Pt 12) (2007) 3308–3320.
- [6] T.G. Hauk, M. Leibinger, A. Müller, A. Andreadaki, U. Knippschild, D. Fischer, Stimulation of axon regeneration in the mature optic nerve by intravitreal application of the toll-like receptor 2 agonist Pam3Cys, *Invest. Ophthalmol. Vis. Sci.* 51 (1) (2010) 459–464.
- [7] M.T. Pardue, R.S. Allen, Neuroprotective strategies for retinal disease, *Prog. Retin. Eye Res.* 65 (2018) 50–76.
- [8] X. Wang, X. Mo, D. Li, Y. Wang, Y. Fang, X. Rong, H. Miao, T. Shou, Neuroprotective effect of transcorneal electrical stimulation on ischemic damage in the rat retina, *Exp. Eye Res.* 93 (5) (2011) 753–760.
- [9] P. Henrich-Noack, E.G. Sergeeva, T. Eber, Q. You, N. Voigt, J. Köhler, S. Wagner, S. Lazik, C. Mawrin, G. Xu, S. Biswas, B.A. Sabel, C.K. Leung, Electrical brain stimulation induces dendritic stripping but improves survival of silent neurons after optic nerve damage, *Sci. Rep.* 7 (1) (2017) 627.
- [10] A. Ashok, W.L. Tai, A. Lennikov, K. Chang, J. Chen, B. Li, K.S. Cho, T.P. Utheim, D. F. Chen, Electrical stimulation alters DNA methylation and promotes neurite outgrowth, *J. Cell Biochem.* 124 (10) (2023) 1530–1545.
- [11] A. Sehic, S. Guo, K.S. Cho, R.M. Corraya, D.F. Chen, T.P. Utheim, Electrical Stimulation as a Means for Improving Vision, *Am. J. Pathol.* 186 (11) (2016) 2783–2797.
- [12] H. Yu, S. Enayati, K. Chang, K. Cho, S.W. Lee, M. Talib, K. Zihlavnikova, J. Xie, H. Achour, S.I. Fried, T.P. Utheim, D.F. Chen, Noninvasive electrical stimulation improves photoreceptor survival and retinal function in mice with inherited photoreceptor degeneration, *Invest. Ophthalmol. Vis. Sci.* 61 (4) (2020) 5.
- [13] K. Chang, S. Enayati, K.S. Cho, T.P. Utheim, D.F. Chen, Non-invasive electrical stimulation as a potential treatment for retinal degenerative diseases, *Neural Regen. Res.* 16 (8) (2021) 1558–1559.
- [14] S. Enayati, K. Chang, A. Lennikov, M. Yang, C. Lee, A. Ashok, F. Elzaridi, C. Yen, K. Gunes, J. Xie, K.S. Cho, T.P. Utheim, D.F. Chen, Optimal transcorneal electrical stimulation parameters for preserving photoreceptors in a mouse model of retinitis pigmentosa, *Neural Regen. Res.* 19 (11) (2024) 2543–2552.
- [15] K. Gunes, K. Chang, A. Lennikov, W.L. Tai, J. Chen, F. Elzaridi, K.S. Cho, T. P. Utheim, Dong Feng C. Preservation of vision by transpalpebral electrical stimulation in mice with inherited retinal degeneration, *Front. Cell Dev. Biol.* 12 (2024) 1412909.
- [16] J. Liu, K. Tong, Y. Lin, V.W.H. Lee, K.F. So, K.C. Shih, J.S.M. Lai, K. Chiu, Effectiveness of microcurrent stimulation in preserving retinal function of blind leading retinal degeneration and optic neuropathy: a systematic review, *Neuromodulation* 24 (6) (2021) 992–1002.
- [17] S. Enayati, K. Chang, H. Achour, K.S. Cho, F. Xu, S. Guo, K. Z. Enayati, J. Xie, E. Zhao, T. Turunen, A. Sehic, L. Lu, T.P. Utheim, D.F. Chen, Electrical stimulation induces retinal müller cell proliferation and their progenitor cell potential, *Cells* 9 (3) (2020) 781.
- [18] B.S. Meldrum, Glutamate as a neurotransmitter in the brain: review of physiology and pathology, *J. Nutr.* 130 (4S Suppl) (2000) 1007S–1015S.
- [19] Y. Okubo, H. Sekiya, S. Namiki, H. Sakamoto, S. Iinuma, M. Yamasaki, M. Watanabe, K. Hirose, M. Iino, Imaging extrasynaptic glutamate dynamics in the brain, *Proc. Natl. Acad. Sci. U S A* 107 (14) (2010) 6526–6531.
- [20] E. Ponomasnik, T. Voyno-Yasenetskaya, D.W. Richter, M. Schachner, A. Dityatev, Morphogenic signaling in neurons via neurotransmitter receptors and small GTPases, *Mol. Neurobiol.* 35 (3) (2007) 278–287.
- [21] M.P. Mattson, Glutamate and neurotrophic factors in neuronal plasticity and disease, *Ann. N. Y. Acad. Sci.* 1144 (2008) 97–112.
- [22] L. Gao, Q.J. Zheng, L.Q. Ai, K.J. Chen, Y.G. Zhou, J. Ye, W. Liu, Exploration of the glutamate-mediated retinal excitotoxic damage: a rat model of retinal neurodegeneration, *Int. J. Ophthalmol.* 11 (11) (2018) 1746–1754.
- [23] J. Lewerenz, P. Maher, Chronic glutamate toxicity in neurodegenerative diseases—what is the evidence? *Front. Neurosci.* 9 (2015) 469.
- [24] Z. Álvarez, O. Castaño, A.A. Castells, M.A. Mateos-Timoneda, J.A. Planell, E. Engel, S. Alcántara, Neurogenesis and vascularization of the damaged brain using a lactate-releasing biomimetic scaffold, *Biomaterials* 35 (17) (2014) 4769–4781.
- [25] K.E. Kador, S.P. Grogan, E.W. Dorthé, P. Venugopalan, M.F. Malek, J.L. Goldberg, D'lima DD, Control of retinal ganglion cell positioning and neurite growth: combining 3d printing with radial electrospun scaffolds, *Tissue Eng. Part A* 22 (3–4) (2016) 286–294.
- [26] C.E. Schmidt, J.B. Leach, Neural tissue engineering: strategies for repair and regeneration, *Annu. Rev. Biomed. Eng.* 5 (2003) 293–347.
- [27] T. Dvir, B.P. Timko, D.S. Kohane, R. Langer, Nanotechnological strategies for engineering complex tissues, *Nat. Nanotechnol.* 6 (1) (2011) 13–22.
- [28] X. Jiang, S.H. Lim, H.Q. Mao, S.Y. Chew, Current applications and future perspectives of artificial nerve conduits, *Exp. Neurol.* 223 (1) (2010) 86–101.
- [29] G.A. Silva, Neuroscience nanotechnology: progress, opportunities and challenges, *Nat. Rev. Neurosci.* 7 (1) (2006) 65–74.
- [30] J. Koffler, W. Zhu, X. Qu, O. Platoshyn, J.N. Dulin, J. Brock, L. Graham, P. Lu, J. Sakamoto, M. Marsala, S. Chen, M.H. Tuszynski, Biomimetic 3D-printed scaffolds for spinal cord injury repair, *Nat. Med.* 25 (2) (2019) 263–269.
- [31] S. Madduri, M. Papaloizos, B. Gander, Trophically and topographically functionalized silk fibroin nerve conduits for guided peripheral nerve regeneration, *Biomaterials* 31 (8) (2010) 2323–2334.
- [32] C.R. Wittmer, T. Claudepierre, M. Reber, P. Wiedemann, J.A. Garlick, D. Kaplan, C. Egles, Multifunctionalized electrospun silk fibers promote axon regeneration in central nervous system, *Adv. Funct. Mater.* 21 (22) (2011) 4202.
- [33] K.E. Kador, R.B. Montero, P. Venugopalan, J. Hertz, A.N. Zindell, D.A. Valenzuela, M.S. Uddin, E.B. Lavik, K.J. Muller, F.M. Andreopoulos, J.L. Goldberg, Tissue

- engineering the retinal ganglion cell nerve fiber layer, *Biomaterials* 34 (17) (2013) 4242–4250.
- [34] Z.H. Wang, Y.Y. Chang, J.G. Wu, C.Y. Lin, H.L. An, S.C. Luo, T.K. Tang, W.F. Su, Novel 3D Neuron Regeneration Scaffolds Based on Synthetic Polypeptide Containing Neuron Cue, *Macromol. Biosci.* 18 (3) (2018).
- [35] C.Y. Lin, S.C. Luo, J.S. Yu, T.C. Chen, W.F. Su, Peptide-Based Polyelectrolyte Promotes Directional and Long Neurite Outgrowth, *ACS Appl. Bio Mater.* 2 (1) (2019) 518–526.
- [36] X. Huang, D.Y. Wu, G. Chen, H. Manji, D.F. Chen, Support of retinal ganglion cell survival and axon regeneration by lithium through a Bcl-2-dependent mechanism, *Invest. Ophthalmol. Vis. Sci.* 44 (1) (2003) 347–354.
- [37] J. Jiao, X. Huang, R.A. Feit-Leithman, R.L. Neve, W. Snider, D.A. Dartt, D.F. Chen, Bcl-2 enhances Ca(2+) signaling to support the intrinsic regenerative capacity of CNS axons, *EMBO J.* 24 (5) (2005) 1068–1078.
- [38] J. Ma, C. Guo, C. Guo, Y. Sun, T. Liao, U. Beattie, F.J. López, D.F. Chen, K. Lashkari, Transplantation of human neural progenitor cells expressing IGF-1 enhances retinal ganglion cell survival, *PLoS One* 10 (4) (2015) e0125695.
- [39] C. Guo, K.S. Cho, Y. Li, K. Tchadre, C. Antolik, J. Ma, J. Chew, T.P. Utheim, X. A. Huang, H. Yu, M.T.A. Malik, N. Anzak, D.F. Chen, IGFBP1 regulates axon growth through IGF-1-mediated signaling cascades, *Sci. Rep.* 8 (1) (2018) 2054.
- [40] A. Meyer-Franke, M.R. Kaplan, F.W. Pfrieger, B.A. Barres, Characterization of the signaling interactions that promote the survival and growth of developing retinal ganglion cells in culture, *Neuron* 15 (4) (1995) 805–819.
- [41] J.L. Goldberg, J.S. Espinosa, Y. Xu, N. Davidson, G.T. Kovacs, B.A. Barres, Retinal ganglion cells do not extend axons by default: promotion by neurotrophic signaling and electrical activity, *Neuron* 33 (5) (2002) 689–702.
- [42] D.F. Chen, G.E. Schneider, J.C. Martinou, S. Tonegawa, Bcl-2 promotes regeneration of severed axons in mammalian CNS, *Nature* 385 (6615) (1997) 434–439.
- [43] M.A. Rogawski, Revisiting AMPA receptors as an antiepileptic drug target, *Epilepsy Curr.* 11 (2) (2011) 56–63.
- [44] A.E. Talpalar, O. Kiehn, Glutamatergic mechanisms for speed control and network operation in the rodent locomotor CpG, *Front. Neural Circuits.* 4 (2010) 19.
- [45] K.S. Cho, D.F. Chen, Promoting optic nerve regeneration in adult mice with pharmaceutical approach, *Neurochem. Res.* 33 (10) (2008) 2126–2133.
- [46] W. Ma, T. Tavakoli, E. Derby, Y. Serebryakova, M.S. Rao, M.P. Mattson, Cell-extracellular matrix interactions regulate neural differentiation of human embryonic stem cells, *BMC. Dev. Biol.* 8 (2008) 90.
- [47] S. Karahuseyinoglu, E. Sekerdag, M.M. Aria, Y. Cetin Tas, S. Nizamoglu, I. Solaroglu, Y. Gürsoy-Özdemir, Three-dimensional neuron-astrocyte construction on matrigel enhances establishment of functional voltage-gated sodium channels, *J. Neurochem.* 156 (6) (2021) 848–866.
- [48] Y.T. Ou, M.S. Lu, C.C. Chiao, The effects of electrical stimulation on neurite outgrowth of goldfish retinal explants, *Brain Res.* 1480 (2012) 22–29.
- [49] M.J. Lee, C.C. Chiao, Short-term alteration of developmental neural activity enhances neurite outgrowth of retinal explants, *Invest. Ophthalmol. Vis. Sci.* 57 (15) (2016) 6496–6506.
- [50] W. Tong, H. Meffin, D.J. Garrett, Ibbotson MR. Stimulation Strategies for Improving the Resolution of Retinal Prostheses, *Front. Neurosci.* 14 (2020) 262.
- [51] I.A. Pearce, M.A. Cambray-Deakin, R.D. Burgoyne, Glutamate acting on NMDA receptors stimulates neurite outgrowth from cerebellar granule cells, *FEBS Lett.* 223 (1) (1987) 143–147.
- [52] F. Metzger, S. Wiese, M. Sendtner, Effect of glutamate on dendritic growth in embryonic rat motoneurons, *J. Neurosci.* 18 (5) (1998) 1735–1742.
- [53] D. Georgiev, H. Taniura, Y. Kambe, T. Takarada, Y. Yoneda, A critical importance of polyamine site in NMDA receptors for neurite outgrowth and fasciculation at early stages of P19 neuronal differentiation, *Exp. Cell Res.* 314 (14) (2008) 2603–2617.
- [54] M.A. Woodruff, D.W. Huttmacher, The return of a forgotten polymer—Polycaprolactone in the 21st century, *Prog. Polym. Sci.* 35 (10) (2010) 1217–1256.
- [55] K. Chen, W. Yu, G. Zheng, Z. Xu, C. Yang, Y. Wang, Z. Yue, W. Yuan, B. Hu, H. Chen, Biomaterial-based regenerative therapeutic strategies for spinal cord injury, *NPG. Asia Mater.* 16 (2024) 5.
- [56] M. Bartnikowski, T.R. Dargaville, S. Ivanovski, D.W. Huttmacher, Degradation mechanisms of polycaprolactone in the context of chemistry, geometry and environment, *Prog. Polym. Sci.* 96 (2019) 1–20.
- [57] J.R. Dias, A. Sousa, A. Augusto, P.J. Bártolo, P.L. Granja, Electrospun Polycaprolactone (PCL) Degradation: an In Vitro and In Vivo Study, *Polym. (Basel)* 14 (16) (2022) 3397.
- [58] M.V. Deshpande, A. Girase, M.W. King, Degradation of poly(ϵ -caprolactone) resorbable multifilament yarn under physiological conditions, *Polym. (Basel)* 15 (18) (2023) 3819.
- [59] G. Feng, R.H. Mellor, M. Bernstein, C. Keller-Peck, Q.T. Nguyen, M. Wallace, J. M. Nerbonne, J.W. Lichtman, J.R. Sanes, Imaging neuronal subsets in transgenic mice expressing multiple spectral variants of GFP, *Neuron* 28 (1) (2000) 41–51.
- [60] A. de Mel, G. Jell, M.M. Stevens, A.M. Seifalian, Biofunctionalization of biomaterials for accelerated in situ endothelialization: a review, *Biomacromolecules* 9 (11) (2008) 2969–2979.
- [61] J.Q. Zheng, J.J. Wan, M.M. Poo, Essential role of filopodia in chemotropic turning of nerve growth cone induced by a glutamate gradient, *J. Neurosci.* 16 (3) (1996) 1140–1149.
- [62] M.P. Mattson, P. Dou, S.B. Kater, Outgrowth-regulating actions of glutamate in isolated hippocampal pyramidal neurons, *J. Neurosci.* 8 (6) (1988) 2087–2100.
- [63] G.J. Brewer, C.W. Cotman, NMDA receptor regulation of neuronal morphology in cultured hippocampal neurons, *Neurosci. Lett.* 99 (3) (1989) 268–273.
- [64] V. De Paola, S. Arber, P. Caroni, AMPA receptors regulate dynamic equilibrium of presynaptic terminals in mature hippocampal networks, *Nat. Neurosci.* 6 (5) (2003) 491–500.
- [65] C.Y. Brazel, J.L. Nuñez, Z. Yang, S.W. Levison, Glutamate enhances survival and proliferation of neural progenitors derived from the subventricular zone, *Neuroscience* 131 (1) (2005) 55–65.
- [66] N. Gogolla, I. Galimberti, P. Caroni, Structural plasticity of axon terminals in the adult, *Curr. Opin. Neurobiol.* 17 (5) (2007) 516–524.
- [67] A. Reiner, J. Levitz, Glutamatergic signaling in the central nervous system: ionotropic and metabotropic receptors in concert, *Neuron* 98 (6) (2018) 1080–1098.
- [68] A.D. Owen, M.M. Bird, Role of glutamate in the regulation of the outgrowth and motility of neurites from mouse spinal cord neurons in culture, *J. Anat.* 191 (Pt 2) (Pt 2) (1997) 301–307.
- [69] P. Chang S De Camilli, Glutamate regulates actin-based motility in axonal filopodia, *Nat. Neurosci.* 4 (8) (2001) 787–793.
- [70] A. Tashiro, A. Dunaevsky, R. Blazeski, C.A. Mason, R. Yuste, Bidirectional regulation of hippocampal mossy fiber filopodial motility by kainate receptors: a two-step model of synaptogenesis, *Neuron* 38 (5) (2003) 773–784.
- [71] G. Ibarretxe, D. Perras, F. Jaskolski, A. Vimeney, C. Mülle, Fast regulation of axonal growth cone motility by electrical activity, *J. Neurosci.* 27 (29) (2007) 7684–7695.
- [72] C.E. Henderson, Role of neurotrophic factors in neuronal development, *Curr. Opin. Neurobiol.* 6 (1) (1996) 64–70.
- [73] C. Deister, C.E. Schmidt, Optimizing neurotrophic factor combinations for neurite outgrowth, *J. Neural Eng.* 3 (2) (2006) 172–179.
- [74] Z. Zhou, P. Yu, H.M. Geller, C.K. Ober, The role of hydrogels with tethered acetylcholine functionality on the adhesion and viability of hippocampal neurons and glial cells, *Biomaterials* 33 (8) (2012) 2473–2481.
- [75] S.Y. Chew, R. Mi, A. Hoke, K.W. Leong, The effect of the alignment of electrospun fibrous scaffolds on Schwann cell maturation, *Biomaterials* 29 (6) (2008) 653–661.
- [76] V.J. Mukhatyar, M. Salmerón-Sánchez, S. Rudra, S. Mukhopadaya, T.H. Barker, A. J. García, R.V. Bellamkonda, Role of fibronectin in topographical guidance of neurite extension on electrospun fibers, *Biomaterials* 32 (16) (2011) 3958–3968.
- [77] J. Xie, W. Liu, M.R. MacEwan, P.C. Bridgman, Y. Xia, Neurite outgrowth on electrospun nanofibers with uniaxial alignment: the effects of fiber density, surface coating, and supporting substrate, *ACS. Nano* 8 (2) (2014) 1878–1885.
- [78] G. Thirivikraman, A. Jagielo, V.K. Lai, S.L. Johnson, M. Keating, A. Nelson, B. Schultz, C.M. Wang, A.J. Levine, E.L. Botvinick, R.T. Tranquillo, Cell contact guidance via sensing anisotropy of network mechanical resistance, *Proc. Natl. Acad. Sci. USA.* 118 (29) (2021) e2024942118.
- [79] D. Shahriari, J.Y. Koffler, M.H. Tuszynski, W.M. Campana, J.S. Sakamoto, Hierarchically ordered porous and high-volume polycaprolactone microchannel scaffolds enhanced axon growth in transected spinal cords, *Tissue Eng. Part A* 23 (9–10) (2017) 415–425.